A Qualitative Assessment of the Multiphase EMMI Plasticity Model Coupled with Phase Transformation Kinetics

Adetokunbo A. Adedoyin

Computer, Computational, and Statistical Sciences Division, Los Alamos National Laboratory, Los Alamos, NM, 87544, USA

Koffi Enakoutsa

Department of Mathematics, California State University, Northridge, 18111 Nordhoff Street, Northridge, CA 91330, USA

Douglas J. Bammann

Mechanical Engineering Department, Mail Stop 9552, 210 Carpenter Building, Mississippi State University, Mississippi State, MS 39762, USA

Abstract

Commonly implemented material processing routines not limited to quenching, welding or heat treatment requires exposure of a part to complex thermal and mechanical loading histories that in turn manifest as residual stress and distortion. Of interest to material designers and fabricators is modeling and simulating the evolutionary process a part undergoes for the sake of capturing this observable residual stress states and geometric distortion accumulated after processing. In an attempt to move toward an overall consistent modeling approach, we premise this investigation with a consistent thermodynamic framework for a generalized multiphase material. Following this, we extend the single phase Evolving Microstructural Model of Inelasticity (EMMI) internal state variable model to multiphase affirming that the interaction between phases is through an interfacial stress. We then employ a self-consistent polycrystalline model in order to partition each individual phase's strain field ensuring a hybrid between compatibility and equilibrium. With a synthesis of the aforementioned ideas, the additional transformation plasticity (TRIP) is accounted for by modifying each phase's flowrule to accommodate an interfacial stress. Following this, we couple the mechanical multiphase model equations with a previously developed non-diffusional phase transformation kinetics model. A numerical evaluation of the coupled model is performed and applied to a simplified quenching boundary value problem.

Keywords: Inelasticity, Continuum Mechanics, Phase Transformation, Kinetics, Thermodynamics

1. Introduction

The pioneering working of Truesdell and Noll [1, 2] on developing, composing and documenting the nonlinear-field theories of mechanics has fostered the extensive application of continuum mathematics to modeling of engineering materials exhibiting non-linear behavior. Subsequent works of Coleman and Noll [3, 4] on finding the restrictions placed on the constitutive formulation designed to account for the dissipative effects expressed through heat conduction and subsequent deformation helped propel the application of thermodynamics to continuum mechanics. Based on the approach taken by [3, 4], Coleman and Gurtin [5] formulated a continuum thermodynamics framework for the application of Internal State Variables (ISVs) to modeling the nonlinear behavior of engineering materials.

The works of Eshelby [6, 7] on determination of the elastic field in and around an ellipsoidal inclusion encouraged the development of view point of a framework for handling materials with discontinuous properties. Further works of Ericksen [8], Ball [9] encouraged the development of an approach to mathematically model the existence of multiphases in an elastic solid. A number of researchers [10, 11] through experimentation, theoretical derivation and calculation have established the fact that martensite develops 24 possible variants in the presence of an austenite phase with each variant showing a distinct lattice orientation.

In the past, several researchers have demonstrated the possibility of extending a continuum mechanics based formulation with ISVs to modeling of co-existing phases. Tanaka and Nagaki [12] devised an approach for modeling engineering materials experiencing phase transition. They introduce two ISVs, one that kept track of crystallographic structure evolution and the other that measures the extent of phase transition. To model the interaction or effects of parent and product phases they introduce a TRIP strain quantity to account for the additional plasticity experienced during phase transformation. In an attempt to capture the plasticity induced as a result of phase transition, Leblond et al. [13, 14] used the Hill-Mandel [15, 16] homogenization process to decompose the macroscopic plastic strain into two contributing portions. They decompose the macroscopic plastic strain into a contribution from classical plasticity and the other from transformation plasticity without a priori assumption of a new microscopic plastic strain.

In an attempt to capture the plasticity induced as a result of phase transition, Leblond et al. [13, 14] via the Hill-Mandel [15, 16] homogenization process decompose the macroscopic plastic strain into two contributing portions. More notably, they decompose the macroscopic plastic strain into a contribution from classical plasticity and the other from transformation plasticity without a priori assumption of a new microscopic plastic strain. In a later work, Leblond et al. [17, 18] experimented with previously proposed relationship between the macroscopic TRIP stain-rate quantity and the stress deviator [19, 20]. Subsequently, neglecting the Magee mechanism [21], they pursued a numerical investigation of the transformation induced plasticity component with a consideration of both perfectly-plastic and strain hardening effects. It is noteworthy to mention that based on experimental observations several other authors [22, 23, 24, 25] had derived constitutive relationships between macroscopic TRIP strain or strain rate and stress analogous to the form of the flow-law for classical plasticity.

Previously, Bammann et al. [26, 27, 28, 29] developed an ISV framework that enabled capturing the temperature and strain rate dependent behavior observable in engineering materials notably the Bammann-Chelsea-Johnson (BCJ) plasticity model. The well established kinematic hardening phenomena was captured using a tensorial state variable where it's rate was cast in a hardening minus recovery format following Ashby [30]. Similarly to the format of the kinematic hardening rate state variable, isotropic hardening rate though a scalar variable, was cast in a hardening minus recovery format. In a subsequent work, Bammann et al. [31] extend the BCJ single phase framework to capture the occurrence of coexisting phase in an engineering material. The effort was directed toward capturing the residual stress and distortion observable in the event of a welding, heat treatment or quenching procedure performed on low alloy steels.

Several finite deformation kinematic frameworks have been proposed to enable capturing the phase transformation phenomena observed in crystalline materials. The more common mathematical framework used to formulate the kinematics of finite deformation for a single phase is based on a multiplicative decomposition of the deformation gradient (F) into an elastic and plastic component. Following Khan [32], the deformation gradient can be decomposed into:

$$\mathbf{F} = \mathbf{F}_e \mathbf{F}_p \tag{1}$$

where $\mathbf{F}_e$ and $\mathbf{F}_p$ is the elastic and plastic part. In a similar manner, this approach has been extended to a multiphase framework. Bock and Holzapfel [33], Kroner [34], and Lee and Liu [35] extended the small strain phase transition framework work earlier developed by Leblond et al. [17, 18] to a large strain framework. They accounted for the additional plasticity relating to the orientation process (Magee Effect) [21].

The evolution law accounting for the TRIP strains was chosen to be of a visco-plastic nature.

More recently, Hallberg et al. [36] using a large-strain plasticity framework proposed a phase transition model to describe martensitic formation in austenitic steels. For the thermodynamic formulation, their choice of state variable included the elastic strain, a hardening variable, temperature and the phase volume fraction of martensite. Using a Crystal plasticity framework, Tjahjanto et al. [37] modeled the Transformation plasticity phenomenon. Based on a finite strain framework they decompose the deformation gradient into:

$$\mathbf{F} = \mathbf{F}_e\mathbf{F}_p\mathbf{F}_{tr} \tag{2}$$

where $\mathbf{F}_e$, $\mathbf{F}_p$ and $\mathbf{F}_{tr}$ is the elastic, plastic and transformation deformation gradient component. A similar model development approach as described above had been taken by numerous authors [38, 39, 40, 41, 42, 43, 44] where the fundamental difference in the model approach may lie in either the TRIP strain formulation and or incorporation, the kinematic assumption, the scale of interest, the choice of internal state variable or the phase evolution kinetics model used.

Continuum mechanics as an approach to modeling and simulating engineering material behavior is attractive. Its mathematical framework enables scientist and engineers capture the behavior of a material in an average manner. Effectively coupling phase kinetics models to a continuum mechanics framework requires several consideration. One of which includes homogeneity, that is, uniform without irregularities, have to be made in order to deem a material point differentiable or continuous where in a numerical sense, the imposed differentiability would allow for a discretizable subset space. It would only be reasonable to assume that each continuum point can readily accommodate evolving new phases. With this approach, phase transformation kinetics can be modeled. Similarly, conservation of energy or similar principles can be estimated as a cumulative sum of each cohabiting phase. In addition, the cumulative stress may then be deduced using a volume fraction weighted rule of mixtures.

Today several researchers are given credit for the development of the equation for modeling the kinetics of phase transformation of a diffusional or non-diffusional type. Common diffusional models are commonly referred to as JMAK after Johnson and Mehl [45], Avarami [46, 47, 48] and Kolmogorov [49]. For a non-diffusional transformation the Koistinen-Marburger [50] model (KM) or some form of it is the most widely adopted model for austenite to martensite transformation. In more recent years, Lusk et al. [51, 52, 53] have experimented with similar approaches to phase transformation kinetics where they premise the development of their model with the balance principle for both diffusional and non-diffusional types. Of consideration here are non-diffusion type models with a focus on low to mild carbon steels.

The rapid development in computer architecture coupled with industrial demand for high resolution and low cost computer simulations has led to the continuous development of numerical tools for simulating heat treatment. Ferguson et al. [54, 55], developed DANTE® a heat treatment subroutine that interfaces with ABAQUS [56]. Using DANTE®, several numerical studies have been conducted in an attempt to better understand the physics of heat treatment and quenching. The development of DANTE® has also fostered collaborative efforts [57, 58, 59, 60]. Other tools such as HEARTS [61, 62], SYSWELD [63] and TRAST [64] have also been developed. The aforementioned tools work as either stand-alone packages or in a plug-in type fashion into well know table-top multi-physics packages like COMSOL [65], ABAQUS [56], SolidWorks [66] and so on.

Motivated by the need to develop a better understanding of heat treatment and quenching of metal alloys, the continuum based EMMI framework has being extended to capture the occurrence of more than a single phase coexisting in a polycrystalline material. Of interest here are materials that undergo phase transformation that consequentially modifies the material mechanical response. Here in we premise this investigation with a consistent thermodynamic framework generalized for n phases. Following this, we extend the single phase EMMI plasticity state variable model to multiphase affirming that the interaction between multiple

phases is through an interface stress. We then employ a self-consistent polycrystalline model to help partition each individual phase's strain field, in a manner where a hybrid between compatibility and equilibrium is satisfied. With a synthesis of the aforementioned ideas, the additional TRIP is numerically accounted for by augmenting each flowrule with the computed interfacial stress. Here we assume a two-phase system and qualitatively associate these phases with martensite and austenite. The transformation kinetics proposed by Lusk [51, 67, 52], as well as some experimental data over a limited strain rate and temperature regime were available to us. The goal of this is to eventually extend this work to all five phases in an attempt to modify and extend the approach taken by Bammann et al. [31, 27, 68, 69]. The following mathematical operations in direct notation are used in the remainder of this paper. They are defined as follows. Given a second rank tensorial quantity $\mathbf{A}$, it follows that $\|\mathbf{A}\| = (\mathbf{A} : \mathbf{A})^{1/2}$, $\mathbf{Tr}\left[\mathbf{A}\right] = (\mathbf{A} : \mathbf{I})^{1/2}$ and $\mathbf{Dev}\left[\mathbf{A}\right] = \acute{\mathbf{A}} = \mathbf{A} - \frac{1}{3}\mathbf{Tr}\left[\mathbf{A}\right]\mathbf{I}$.

2. Methodology

2.1. Multiphase Modeling - Thermodynamic arguments for a multiphase polycrystalline material

The formulation of the model follows the general thermodynamic formulation proposed by Bammann [70, 71]. The deformation or strain is decomposed into a lattice strain (which is further decomposed into strains in each component if multiple phases are present), the interface between phases, and the elastic strain associated with each defect densities in each phases. Therefore, given a body consisting of n phases, the strain components are:

$$\boldsymbol{\epsilon} \supset \left\{\boldsymbol{\epsilon}_l^{(i)}, \boldsymbol{\epsilon}_{ss}^{(i)}, \boldsymbol{\epsilon}_\beta^{(i)}, \boldsymbol{\epsilon}_\pi\right\} \tag{3}$$

where $\boldsymbol{\epsilon}_l^{(i)}$ is the lattice strain in the each phase. $\boldsymbol{\epsilon}_{ss}^{(i)}$ is the strain resulting from statistically stored dislocations (SSDs) in the each phase. $\boldsymbol{\epsilon}_\beta^{(i)}$ is the strain resulting from geometrically necessary dislocations (GNDs) in the each phase. $\boldsymbol{\epsilon}_\pi$ is the interface strain between phases. The superscript i is a range variable representing each phase where the symbol n represents the total number of phases under consideration. Furthermore, each of these strains is decomposed into elastic and inelastic (plastic) parts, such that:

$$\underbrace{\boldsymbol{\epsilon}_l^{(i)} = \left(\boldsymbol{\epsilon}_{l,e}^{(i)} + \boldsymbol{\epsilon}_{l,p}^{(i)}\right)}_{lattice} \quad \underbrace{\boldsymbol{\epsilon}_\beta^{(i)} = \left(\boldsymbol{\epsilon}_{\beta,e}^{(i)} + \boldsymbol{\epsilon}_{\beta,p}^{(i)}\right)}_{GNDs} \quad \underbrace{\boldsymbol{\epsilon}_{ss}^{(i)} = \left(\boldsymbol{\epsilon}_{ss,e}^{(i)} + \boldsymbol{\epsilon}_{ss,p}^{(i)}\right)}_{SSDs} \quad \underbrace{\boldsymbol{\epsilon}_\pi = \left(\boldsymbol{\epsilon}_{\pi,e} + \boldsymbol{\epsilon}_{\pi,p}\right)}_{interface}. \tag{4}$$

From the second law of thermodynamics, the reduced entropy inequality is:

$$\dot{\psi} \leq W_{total} \tag{5}$$

where W_{total} represents the total work done. Similar to the thermodynamics proposed by Gurtin [72], for a single phase material the right hand side of the inequality represents the total work done comprising of macroscopic and microscopic:

$$\dot{\psi} \leq W_{macro} + W_{micro}. \tag{6}$$

The composition of the macroscopic work is:

$$W_{macro} = \underbrace{\sum_{i=1}^{n} \boldsymbol{\sigma}^{(i)} : \left(\dot{\boldsymbol{\epsilon}}_l^{(i)} + \dot{\boldsymbol{\epsilon}}_\beta^{(i)} + \dot{\boldsymbol{\epsilon}}_{ss}^{(i)} + \dot{\boldsymbol{\epsilon}}_\pi\right)}_{total\ marcro\ work} \quad \rightarrow \quad \sum_{i=1}^{n} \boldsymbol{\sigma}^{(i)} : \left(\dot{\boldsymbol{\epsilon}}_l^{(i)}\right) + \underbrace{\sum_{i=1}^{n} \boldsymbol{\sigma}^{(i)} : \left(\dot{\boldsymbol{\epsilon}}_\beta^{(i)} + \dot{\boldsymbol{\epsilon}}_{ss}^{(i)} + \dot{\boldsymbol{\epsilon}}_\pi\right)}_{cross\ components} \tag{7}$$

where $\boldsymbol{\sigma}^{(i)}$ is the macroscopic Cauchy stress operating on each component of strain in a multiphase body. The microscopic work comprises of:

$$W_{micro} = \underbrace{\boldsymbol{\pi} : \dot{\boldsymbol{\epsilon}}_\pi}_{interface\ work} + \underbrace{\sum_{i=1}^{n} \left[\boldsymbol{\alpha}^{(i)} : \left(\dot{\boldsymbol{\epsilon}}_\beta^{(i)}\right) + \boldsymbol{\kappa}^{(i)} : \left(\dot{\boldsymbol{\epsilon}}_{ss}^{(i)}\right)\right]}_{micro\text{-}stress\ work} \tag{8}$$

where $\boldsymbol{\pi}$ is the tensorial interface stress between phases. $\boldsymbol{\kappa}^{(i)}$ is the tensorial stress like internal state variable serving as a work conjugate pair to the straining $\boldsymbol{\epsilon}_{ss}^{(i)}$ associated with the SSDs in each phase. $\boldsymbol{\alpha}^{(i)}$ is the tensorial stress like internal state variable serving as a work conjugate pair to the straining $\boldsymbol{\epsilon}_{\beta}^{(i)}$ associated with the GNDs in each phase. At this point, we assume that ($\boldsymbol{\epsilon}_{ss}^{(i)}$) the SSDs strain reduces to a scalar measure of the elastic strain in a dislocation array. In that case, for a polycrystalline material $\boldsymbol{\epsilon}_{ss}^{(i)}$ averages to the same value in all directions; similar to the concept of isotropic hardening in classical plasticity. Similarly, we treat the interfacial stress in the same manner as the as acting in a non-directional manner. In a future work, we will utilize an orientation tensor to introduce the directionality of the tensorial interfacial π stress into the model, naturally incorporating the shearing aspects of the transformation process. In addition, we would neglect cross terms between stresses and strain rates. With this assumption, a given a body consisting of two phases, austenite and martensite, the macroscopic work simplifies to:

$$W_{macro} = \underbrace{\sum_{i=1}^{2} \boldsymbol{\sigma}^{(i)} : \left(\dot{\boldsymbol{\epsilon}}_{l}^{(i)}\right)}_{\textit{approx. total marcro work}}. \tag{9}$$

Following the aforementioned assumptions the microscopic work reduces to:

$$W_{micro} = \underbrace{\pi\dot{\epsilon}_{\pi} + \sum_{i=1}^{2} \left[\kappa^{(i)}\left(\dot{\epsilon}_{ss}^{(i)}\right) + \boldsymbol{\alpha}^{(i)} : \left(\dot{\boldsymbol{\epsilon}}_{\beta}^{(i)}\right)\right]}_{\textit{approx. total micro work}}. \tag{10}$$

Following the approach introduced by Coleman and Noll [3] in an attempt to determine the logical connection between the principles of conservation of energy, entropy inequality and the general principles in mechanics, Coleman and Gurtin [5] determined the thermodynamic restrictions necessary when introducing ISVs to a continuum mechanics framework. In the same light we argue that, the Helmholtz free energy is of the form:

$$\psi = e - \theta\eta \tag{11}$$

where e is the internal energy, θ represents temperature and η the entropy. In rate form the Helmholtz free energy is:

$$\dot{\psi} = \dot{e} - \dot{\theta}\eta - \theta\dot{\eta}. \tag{12}$$

If we assume isothermal conditions, the rate form of the Helmholtz free energy reduces to:

$$\dot{\psi} = \dot{e} - \theta\dot{\eta}. \tag{13}$$

Substituting Eqn. (9) and Eqn. (10) into Eqn. (6) gives:

$$\dot{\psi} \leq \underbrace{\pi\dot{\epsilon}_{\pi} + \sum_{i=1}^{2} \left[\boldsymbol{\sigma}^{(i)} : \left(\dot{\boldsymbol{\epsilon}}_{l}^{(i)}\right) + \boldsymbol{\alpha}^{(i)} : \left(\dot{\boldsymbol{\epsilon}}_{\beta}^{(i)}\right) + \kappa^{(i)}\left(\dot{\epsilon}_{ss}^{(i)}\right)\right]}_{\textit{approx. total work}}. \tag{14}$$

Furthermore, decomposing each of these strains into elastic and inelastic or plastic parts, Eqn. (14) becomes:

$$\dot{\psi} \leq \underbrace{\pi\left[\dot{\epsilon}_{\pi,e} + \dot{\epsilon}_{\pi,p}\right]}_{\textit{total interface work}} + \sum_{i=1}^{2} \left[\underbrace{\boldsymbol{\sigma}^{(i)} : \left[\dot{\boldsymbol{\epsilon}}_{l,e}^{(i)} + \dot{\boldsymbol{\epsilon}}_{l,p}^{(i)}\right]}_{\textit{total external work}} + \underbrace{\boldsymbol{\alpha}^{(i)} : \left[\dot{\boldsymbol{\epsilon}}_{\beta,e}^{(i)} + \dot{\boldsymbol{\epsilon}}_{\beta,p}^{(i)}\right] + \kappa^{(i)}\left[\dot{\epsilon}_{ss,e}^{(i)} + \dot{\epsilon}_{ss,p}^{(i)}\right]}_{\textit{total internal work}}\right]. \tag{15}$$

Assuming that no inelastic deformation occurs, at the interface, Eqn. (15) becomes:

$$\dot{\psi} \leq \pi\left[\dot{\epsilon}_{\pi,e}\right] + \sum_{i=1}^{2} \left[\boldsymbol{\sigma}^{(i)} : \left[\dot{\boldsymbol{\epsilon}}_{l,e}^{(i)} + \dot{\boldsymbol{\epsilon}}_{l,p}^{(i)}\right] + \boldsymbol{\alpha}^{(i)} : \left[\dot{\boldsymbol{\epsilon}}_{\beta,e}^{(i)} + \dot{\boldsymbol{\epsilon}}_{\beta,p}^{(i)}\right] + \kappa^{(i)}\left[\dot{\epsilon}_{ss,e}^{(i)} + \dot{\epsilon}_{ss,p}^{(i)}\right]\right]. \tag{16}$$

We assume that the Helmholtz free energy depends on a number of independent state variables namely the elastic portion of the lattice strain in each phase $\boldsymbol{\epsilon}_{l,e}^{(i)}$, the elastic strain like internal state variable due to SSDs and GNDs $\epsilon_{ss,e}^{(i)}$ and $\boldsymbol{\epsilon}_{\beta,e}^{(i)}$ and the elastic interfacial strain $\epsilon_{\pi,e}$. We further represent each category of state variables in each phase as:

$$\underbrace{\mathbf{Z}_{l,e} \Rightarrow \left\{\boldsymbol{\epsilon}_{l,e}^{(1)}, \boldsymbol{\epsilon}_{l,e}^{(2)}\right\}}_{lattice} \quad \underbrace{\mathbf{Z}_{\beta,e} \Rightarrow \left\{\boldsymbol{\epsilon}_{\beta,e}^{(1)}, \boldsymbol{\epsilon}_{\beta,e}^{(2)}\right\} \qquad Z_{ss,e} \Rightarrow \left\{\epsilon_{ss,e}^{(1)}, \epsilon_{ss,e}^{(2)}\right\}}_{internal\ elastic\ strain\ fields} \qquad \underbrace{Z_{\pi,e} \Rightarrow \{\epsilon_{\pi,e}\}}_{internal\ elastic\ interface} . \tag{17}$$

Therefore the Helmholtz free energy is further expressed as dependent on:

$$\psi = \hat{\psi}\left(\mathbf{Z}_{l,e}, \mathbf{Z}_{\beta,e}, Z_{ss,e}, Z_{\pi,e}\right). \tag{18}$$

Applying the chain rule to Eqn. (18) yields:

$$\dot{\psi} = \sum_{i=1}^{2}\left[\frac{\partial \psi}{\partial \boldsymbol{\epsilon}_{l,e}^{(i)}} : \dot{\boldsymbol{\epsilon}}_{l,e}^{(i)} + \frac{\partial \psi}{\partial \boldsymbol{\epsilon}_{\beta,e}^{(i)}} : \dot{\boldsymbol{\epsilon}}_{\beta,e}^{(i)} + \frac{\partial \psi}{\partial \epsilon_{ss,e}^{(i)}}\dot{\epsilon}_{ss,e}^{(i)}\right] + \frac{\partial \psi}{\partial \epsilon_{\pi,e}}\dot{\epsilon}_{\pi,e}. \tag{19}$$

Substituting Eqn. (19) into Eqn. (16) and further expanding:

$$\begin{aligned}\sum_{i=1}^{2}\left[\frac{\partial \psi}{\partial \boldsymbol{\epsilon}_{l,e}^{(i)}} : \dot{\boldsymbol{\epsilon}}_{l,e}^{(i)} + \frac{\partial \psi}{\partial \boldsymbol{\epsilon}_{\beta,e}^{(i)}} : \dot{\boldsymbol{\epsilon}}_{\beta,e}^{(i)} + \frac{\partial \psi}{\partial \epsilon_{ss,e}^{(i)}}\dot{\epsilon}_{ss,e}^{(i)}\right] + \frac{\partial \psi}{\partial \epsilon_{\pi,e}}\dot{\epsilon}_{\pi,e} \leq \\ \sum_{i=1}^{2}\left[\boldsymbol{\sigma}^{(i)} : \left(\dot{\boldsymbol{\epsilon}}_{l,e}^{(i)} + \dot{\boldsymbol{\epsilon}}_{l,p}^{(i)}\right) + \boldsymbol{\alpha}^{(i)} : \left(\dot{\boldsymbol{\epsilon}}_{\beta,e}^{(i)} + \dot{\boldsymbol{\epsilon}}_{\beta,p}^{(i)}\right) + \kappa^{(i)}\left(\dot{\epsilon}_{ss,e}^{(i)} + \dot{\epsilon}_{ss,p}^{(i)}\right)\right] + \pi\left(\dot{\epsilon}_{\pi,e}\right).\end{aligned} \tag{20}$$

Employing the Coleman and Noll [3] argument and grouping yields:

$$\begin{aligned}\sum_{i=1}^{2}\left[\left[\frac{\partial \psi}{\partial \boldsymbol{\epsilon}_{l,e}^{(i)}} - \boldsymbol{\sigma}^{(i)}\right] : \dot{\boldsymbol{\epsilon}}_{l,e}^{(i)} + \left[\frac{\partial \psi}{\partial \boldsymbol{\epsilon}_{\beta,e}^{(i)}} - \boldsymbol{\alpha}^{(i)}\right] : \dot{\boldsymbol{\epsilon}}_{\beta,e}^{(i)} + \left[\frac{\partial \psi}{\partial \epsilon_{ss,e}^{(i)}} - \kappa^{(i)}\right]\dot{\epsilon}_{ss,e}^{(i)}\right] + \left[\frac{\partial \psi}{\partial \epsilon_{\pi,e}} - \pi\right]\dot{\epsilon}_{\pi,e} \leq \\ \sum_{i=1}^{2}\left[\boldsymbol{\sigma}^{(i)} : \left(\dot{\boldsymbol{\epsilon}}_{l,p}^{(i)}\right) + \boldsymbol{\alpha}^{(i)} : \left(\dot{\boldsymbol{\epsilon}}_{\beta,p}^{(i)}\right) + \kappa^{(i)}\left(\dot{\epsilon}_{ss,p}^{(i)}\right)\right].\end{aligned} \tag{21}$$

Therefore as the elastic strains vanish the stresses and internal state variables associated with each phase is:

$$\begin{aligned}&\underbrace{\boldsymbol{\sigma}^{(1)} = \frac{\partial \psi}{\partial \boldsymbol{\epsilon}_{l,e}^{(1)}}, \quad \boldsymbol{\sigma}^{(2)} = \frac{\partial \psi}{\partial \boldsymbol{\epsilon}_{l,e}^{(2)}},}_{lattice} \quad \underbrace{\boldsymbol{\alpha}^{(1)} = \frac{\partial \psi}{\partial \boldsymbol{\epsilon}_{\alpha,e}^{(1)}}, \quad \boldsymbol{\alpha}^{(2)} = \frac{\partial \psi}{\partial \boldsymbol{\epsilon}_{\alpha,e}^{(2)}},}_{GNDs} \\ &\underbrace{\kappa^{(1)} = \frac{\partial \psi}{\partial \dot{\epsilon}_{ss,e}^{(2)}}, \quad \kappa^{(2)} = \frac{\partial \psi}{\partial \dot{\epsilon}_{ss,e}^{(2)}},}_{SSDs} \quad \underbrace{\pi = \frac{\partial \psi}{\partial \epsilon_{\pi,e}}.}_{interface}\end{aligned} \tag{22}$$

The dissipation inequality becomes:

$$\underbrace{\sum_{i=1}^{2}\left[\boldsymbol{\sigma}^{(i)} : \left[\dot{\boldsymbol{\epsilon}}_{l,p}^{(i)}\right] + \boldsymbol{\alpha}^{(i)} : \left[\dot{\boldsymbol{\epsilon}}_{\beta,p}^{(i)}\right] + \kappa^{(i)}\left[\dot{\epsilon}_{ss,p}^{(i)}\right]\right]}_{plastic\ dissipation} \geq 0 \tag{23}$$

2.2. Multiphase Modeling - Multiphase EMMI Constitutive Equations

In order to extend the EMMI model to capture the physics of materials undergoing phase transformation, while the dislocation based internal state variable (ISV) model is developed for finite strain, the assumption that each continuum point is occupied by both a parent and a product phase had to be made. Using a volume fraction weighted rule of mixtures the Cauchy stress in the current configuration is determined to be of the form:

$$\boldsymbol{\sigma} = \sum_{i=1}^{n} \phi^{(i)} \boldsymbol{\sigma}^{(i)} \tag{24}$$

where $\acute{\boldsymbol{\sigma}}^{(i)}$ represents the Cauchy stress in each phase and the superscript indicate the i^{th} phase. Subsequent volume fraction ($\phi^{(i)}$) are given by:

$$\phi^{(i)} = (1 - \sum_{j \neq i}^{n} \phi^{(j)}). \tag{25}$$

Here we assume a two-phase system and qualitatively associate these phases with austenite and martensite. Therefore the Cauchy stress reduces to:

$$\boldsymbol{\sigma} = \underbrace{\phi^{(1)}\boldsymbol{\sigma}^{(1)} + \phi^{(2)}\boldsymbol{\sigma}^{(2)}}_{\textit{total stress}} \quad \rightarrow \quad \boldsymbol{\sigma} = \underbrace{(1-\phi)\,\boldsymbol{\sigma}^{(1)}}_{\textit{austenite}} + \underbrace{\phi\boldsymbol{\sigma}^{(2)}}_{\textit{martensite}} \tag{26}$$

where $\phi^{(1)}$ and $\phi^{(2)}$ represents the volume fraction of the austenite and martensite and therefore can be mathematically replaced by $1 - \phi$ and ϕ. From the assumption of linear elasticity, and for a homogeneous isotropic material, the deviatoric stress and pressure in each phase is given by:

$$\overset{\circ}{\acute{\boldsymbol{\sigma}}}^{(i)} = \underbrace{\left(\frac{\acute{\boldsymbol{\sigma}}^{(i)}}{\mu^{(i)}}\frac{d\mu^{(i)}}{d\theta}\right)\dot{\theta} + 2\mu^{(i)}\acute{\mathbf{d}}_e^{(i)}}_{\textit{deviatoric stress rate}} \qquad \dot{\mathbf{p}}^{(i)} = \underbrace{\left(\frac{\mathbf{p}^{(i)}}{\kappa^{(i)}}\frac{d\kappa^{(i)}}{d\theta}\right)\dot{\theta} + \kappa^{(i)}\mathbf{Tr}\left[\mathbf{d}_e^{(i)}\right]\mathbf{I}}_{\textit{hydrostatic stress rate}} \tag{27}$$

where $\mu^{(i)}$ and $\kappa^{(i)}$ represent the temperature dependent shear and bulk modulus for each phase. $\theta^{(i)}$ is the temperature in each phase. $\acute{\mathbf{d}}_e^{(i)}$ is the deviatoric elastic part of the symmetrical portion of the velocity gradient in each phase. $\mathbf{I}$ is the three dimensional identity tensor. The convective derivative of the Cauchy stress is of the form:

$$\overset{\circ}{\boldsymbol{\sigma}}^{(i)} = \dot{\boldsymbol{\sigma}}^{(i)} - \mathbf{w}_e^{(i)}\boldsymbol{\sigma}^{(i)} + \boldsymbol{\sigma}^{(i)}\mathbf{w}_e^{(i)} \tag{28}$$

where $\mathbf{w}_e^{(i)}$ is the elastic part of the asymmetrical portion of the velocity gradient in each phase. The elastic symmetrical and asymmetrical portions of the velocity gradient in each phase are respectively:

$$\mathbf{d}_e^{(i)} = \underbrace{\mathbf{d}^{(i)} - \mathbf{d}_p^{(i)} - \mathbf{d}_\theta^{(i)}}_{sym(l_e)} \qquad \mathbf{w}_e^{(i)} = \underbrace{\mathbf{w}^{(i)} - \mathbf{w}_p^{(i)} - \mathbf{w}_\theta^{(i)}}_{asym(l_e)} \tag{29}$$

where the total, plastic and thermal parts of the symmetrical portion of the velocity gradient in each phase is $\mathbf{d}^{(i)}$, $\mathbf{d}_p^{(i)}$ and $\mathbf{d}_\theta^{(i)}$, respectively. Similarly the total, plastic and thermal parts of the asymmetrical portion of the velocity gradient in each phase is $\mathbf{w}^{(i)}$, $\mathbf{w}_p^{(i)}$ and $\mathbf{w}_\theta^{(i)}$, respectively. The partitioning of the total velocity gradient based on it's constituent spin and stretch is will be dependent on the polycrystalline model chosen. The form of the temperature dependent portion of each material property was chosen following the approach taken by Marin et al. [73]. The shear modulus ($\mu^{(i)}$) in each phase is defined as:

$$\mu^{(i)} = \mu_0^{(i)}\hat{\mu}\,(\theta)^{(i)} \tag{30}$$

where $\mu_0^{(i)}$ is the shear modulus at room temperature in each phase. $\hat{\mu}\,(\theta)^{(i)}$ is the functional form of the temperature dependence of the shear modulus. Following Frost and Ashby [74] the definition of the temperature dependence is:

$$\hat{\mu}\,(\theta)^{(i)} = 1 + c_{\theta\mu}^{(i)}\left(\frac{\theta - \theta_0^{(i)}}{\theta_m^{(i)}}\right) \qquad c_{\theta\mu}^{(i)} = \frac{\theta_m^{(i)}}{\mu_0^{(i)}}\frac{d\mu^{(i)}}{d\theta} < 0 \tag{31}$$

θ represents the temperature of the material. $\theta_0^{(i)}$ represents the reference temperature in each phase. θ_m represents the melt temperature in each phase. Similarly, the bulk modulus $\kappa^{(i)}$ is defined as:

$$\kappa^{(i)} = \kappa_0^{(i)} \hat{\kappa}(\theta)^{(i)} \tag{32}$$

where $\kappa_0^{(i)}$ is the bulk modulus at room temperature in each phase. $\hat{\kappa}(\theta)^{(i)}$ is the functional form of the temperature dependence of the bulk modulus. Following Frost and Ashby [74] the definition of the temperature dependence of the bulk modulus is:

$$\hat{\kappa}(\theta)^{(i)} = 1 + c_{\theta\kappa}^{(i)} \left(\frac{\theta^{(i)} - \theta_0^{(i)}}{\theta_m^{(i)}} \right) \qquad c_{\theta\kappa}^{(i)} = \frac{\theta_m^{(i)}}{\kappa_0^{(i)}} \frac{d\kappa^{(i)}}{d\theta} < 0 \tag{33}$$

similarly, θ represents the temperature of the material. $\theta_0^{(i)}$ represents the reference temperature in each phase. θ_m represents the melt temperature in each phase. The tensorial internal state variables $\boldsymbol{\alpha}^{(i)}$ is of the form:

$$\boldsymbol{\alpha}^{(i)} = 2\mu^{(i)} c_\alpha^{(i)} \boldsymbol{\epsilon}_\beta^{(i)} \tag{34}$$

where $\mu^{(i)}$ is the temperature dependent shear modulus in each phase. $\boldsymbol{\epsilon}_\beta^{(i)}$ is the straining associated with GNDs in each phase. $c_\alpha^{(i)}$ is a dimensionless material parameter associated with each phase. In rate form $\boldsymbol{\alpha}^{(i)}$ in each phase is:

$$\dot{\boldsymbol{\alpha}}^{(i)} = \frac{\boldsymbol{\alpha}}{\mu^{(i)}} \dot{\mu}^{(i)} + 2\mu^{(i)} c_\alpha^{(i)} \dot{\boldsymbol{\epsilon}}_\beta^{(i)} \tag{35}$$

The tensorial rate form of the straining associated with GNDs density in each phase is determined to be in a hardening minus recovery format following Armstrong and Frederick [75]:

$$\dot{\boldsymbol{\epsilon}}_\beta^{(i)} = \left(\underbrace{h^{(i)} \acute{\mathbf{N}}^{(i)}}_{\textit{hardening}} - \underbrace{r_d^{(i)} \sqrt{\frac{2}{3}} \boldsymbol{\epsilon}_\beta^{(i)} \left\| \boldsymbol{\epsilon}_\beta^{(i)} \right\|}_{\textit{dynamic recovery}} \right) \dot{\bar{\epsilon}}_p^{(i)} \tag{36}$$

Substituting Eqn. (34) into Eqn. (36) gives the evolution equation for $\boldsymbol{\alpha}$ (Eqn. (37)):

$$\mathring{\boldsymbol{\alpha}}^{(i)} = \left(\frac{\boldsymbol{\alpha}^{(i)}}{\mu^{(i)}} \frac{d\mu^{(i)}}{d\theta} \right) \dot{\theta} + \left(3\mu^{(i)} c_{\boldsymbol{\alpha}}^{(i)} h^{(i)} \acute{\mathbf{N}}^{(i)} - \frac{r_d^{(i)}}{2\mu^{(i)} c_{\boldsymbol{\alpha}}^{(i)}} \sqrt{\frac{2}{3}} \left\| \boldsymbol{\alpha}^{(i)} \right\| \boldsymbol{\alpha}^{(i)} \right) \dot{\bar{\epsilon}}_p^{(i)} \tag{37}$$

where $h^{(i)}$ the hardening parameter in each phase. $r_d^{(i)}(\theta)$ is the temperature dependent dynamic recovery parameter in each phase. $\dot{\bar{\epsilon}}_p^{(i)}$ is the net effective plastic strain rate. The convective derivative of the kinematic state variable is of the form:

$$\mathring{\boldsymbol{\alpha}}^{(i)} = \dot{\boldsymbol{\alpha}}^{(i)} - \mathbf{w}_e^{(i)} \boldsymbol{\alpha}^{(i)} + \boldsymbol{\alpha}^{(i)} \mathbf{w}_e^{(i)} \tag{38}$$

Following the assumption that the SSDs strain ($\boldsymbol{\epsilon}_{ss}^{(i)}$) reduces to a scalar measure of the elastic strain in a dislocation array, for a polycrystalline material it mathematically implies that $\boldsymbol{\epsilon}_{ss}^{(i)}$ averages to the same value in all directions; similar to the concept of isotropic hardening in classical plasticity. Therefore the stress like internal state variable $\kappa^{(i)}$, the work conjugate pair to the straining $\epsilon_{ss}^{(i)}$ associated with the SSDs in each phase reduces to a scalar chosen to be of the form:

$$\kappa^{(i)} = 2\mu^{(i)} c_\kappa^{(i)} \epsilon_{ss}^{(i)} \tag{39}$$

where $\mu^{(i)}$ is the temperature dependent shear modulus. $\epsilon_{ss}^{(i)}$ is the straining associated with SSDs. $c_\kappa^{(i)}$ is the dimensionless material parameter associated with each phase. In rate form $\kappa^{(i)}$ is:

$$\dot{\kappa}^{(i)} = \frac{\kappa}{\mu^{(i)}} \dot{\mu}^{(i)} + 2\mu^{(i)} c_\kappa^{(i)} \dot{\epsilon}_{ss}^{(i)} \tag{40}$$

The mathematical definition of $\epsilon_{ss}^{(i)}$ in each phase is:

$$\epsilon_{ss}^{(i)} = b^{(i)} \sqrt{\rho_{ss}^{(i)}} \tag{41}$$

where $b^{(i)}$ is the magnitude of the burger and $\rho_{ss}^{(i)}$ is the dislocation density of SSDs. The rate form the SSDs density is:

$$\dot{\epsilon}_{ss}^{(i)} = \underbrace{\dot{b}^{(i)} \sqrt{\rho_{ss}^{(i)}}}_{negligible} + b^{(i)} \sqrt[-1]{4\rho_{ss}^{(i)}} \dot{\rho}_{ss}^{(i)} \quad \rightarrow \quad \dot{\epsilon}_{ss}^{(i)} = b^{(i)} \sqrt[-1]{4\rho_{ss}^{(i)}} \dot{\rho}_{ss}^{(i)} \tag{42}$$

The form of the evolution law for $\dot{\rho}_{ss}^{(i)}$ as determined by Kock and Mecking [76] and Estrin and Mecking [77] accounting for thermally activated hardening and dynamic recovery of SSDs, in each phase is:

$$\dot{\rho}_{ss}^{(i)} = \left(\underbrace{c_1^{(i)} \sqrt{\rho_{ss}^{(i)}}}_{hardening} - \underbrace{c_2^{(i)}(\theta) \rho_{ss}^{(i)}}_{dynamic\ recovery} \right) \dot{\bar{\epsilon}}_p^{(i)} \tag{43}$$

where $\dot{\bar{\epsilon}}_p^{(i)}$ is the effective plastic strain rate in each phase. $c_1^{(i)}$ and $c_2^{(i)}$ are material parameters in each phase determined using experimental data. The static recovery component of $\dot{\rho}_{ss}^{(i)}$ accounting for thermal diffusion of dislocations as determined by Nes [78] is of the form:

$$\dot{\rho}_{ss}^{(i)} = \underbrace{-c_3^{(i)}(\theta) \rho_{ss}^{(i)} \sinh \left[c_4^{(i)}(\theta) \sqrt{\rho_{ss}^{(i)}} \right]}_{static\ recovery} \tag{44}$$

where $c_3^{(i)}$ and $c_4^{(i)}$ are material parameters associated with each phase determined using experimental data. In full form, the SSDs density rate $\dot{\rho}_{ss}^{(i)}$ accounting for thermal diffusion of dislocations and thermally activated hardening and dynamic recovery is:

$$\dot{\rho}_{ss}^{(i)} = \left(c_1^{(i)} \sqrt{\rho_{ss}^{(i)}} - c_2^{(i)}(\theta) \rho_{ss}^{(i)} \right) \dot{\bar{\epsilon}}_p^{(i)} - c_3^{(i)}(\theta) \rho_{ss}^{(i)} \sinh \left[c_4^{(i)}(\theta) \sqrt{\rho_{ss}^{(i)}} \right] \tag{45}$$

Substituting Eqn. (40), Eqn. (41) and Eqn. (42) into Eqn. (45) gives the evolution equation for κ (Eqn. (46)):

$$\dot{\kappa}^{(i)} = \left(\frac{\kappa^{(i)}}{\mu^{(i)}} \frac{d\mu^{(i)}}{d\theta} \right) \dot{\theta} + \left(2\mu^{(i)} H^{(i)} c_k^{(i)} \right) \dot{\bar{\epsilon}}_p^{(i)} - \left(R_d^{(i)} \dot{\bar{\epsilon}}_p^{(i)} + R_s^{(i)} \sinh \left[\frac{Q_s^{(i)} \kappa^{(i)}}{2\mu^{(i)} c_k^{(i)}} \right] \right) \kappa^{(i)} \tag{46}$$

where $H^{(i)}$ is the hardening parameter in each phase. $R_s^{(i)}(\theta)$ and $R_d^{(i)}(\theta)$ are the static and dynamic recovery parameter associated with each phase. $c_k^{(i)}$ is the dimensionless isotropic parameter in each phase. The constitutive equation governing plastic flow is presumed to be of the form:

$$\mathbf{d}_p^{(i)} = \sqrt{\frac{3}{2}} \dot{\bar{\epsilon}}_p^{(i)} \acute{\mathbf{N}}^{(i)} \tag{47}$$

where $\acute{\mathbf{N}}$ is the normalized deviatoric tensorial quantity dictating direction of plastic flow in each phase given by:

$$\acute{\mathbf{N}}^{(i)} = \frac{\acute{\boldsymbol{\xi}}^{(i)}}{\left\| \acute{\boldsymbol{\xi}}^{(i)} \right\|} \qquad \left\| \acute{\boldsymbol{\xi}}^{(i)} \right\| = \left\| \acute{\boldsymbol{\sigma}}^{(i)} - \tfrac{2}{3} \acute{\boldsymbol{\alpha}}^{(i)} \right\| \tag{48}$$

The effective plastic flow ($\dot{\bar{\epsilon}}_p^{(i)}$) in each phase given by:

$$\dot{\bar{\epsilon}}_p^{(i)} = f^{(i)} \sinh \left[\frac{\sqrt{\frac{3}{2}} \left\| \acute{\boldsymbol{\xi}}^{(i)} \right\| \pm \pi^{(i)}}{\kappa^{(i)} + Y^{(i)}(\theta)} - 1 \right]^{n^{(i)}} \tag{49}$$

where $f^{(i)}$ the transition parameter in each phase. $n^{(i)}$ is the plastic exponent in each phase. $Y^{(i)}$ is the temperature dependent yield strength in each phase given by:

$$Y^{(i)} = 2\mu_0^{(i)} c_8^{(i)} \hat{Y}\,(\theta)^{(i)} \tag{50}$$

where $c_8^{(i)}$ is the yield parameter in each phase fitted to experimental data. $\hat{Y}^{(i)}(\theta)$ is the temperature dependent portion of the yield strength in each phase assumed to be of the form:

$$\hat{Y}\,(\theta)^{(i)} = \left[\frac{m_1^{(i)}}{1 + m_2^{(i)} \exp\left(\frac{-m_3^{(i)}}{\theta}\right)}\right] \frac{1}{2}\left[1 + \tanh\left(m_4^{(i)}(m_5^{(i)} - \theta)\right)\right]. \tag{51}$$

The thermal part of the symmetric portion of the velocity gradient in each phase is given by:

$$\mathbf{d}_\theta^{(i)} = \dot{\epsilon}_\theta^{(i)} \mathbf{I}. \tag{52}$$

$\dot{\epsilon}_\theta^{(i)}$ represents the thermal elastic strain rate due to result of thermal expansion and contraction in each phase is given by:

$$\dot{\epsilon}_\theta^{(i)} = f_\beta\,(\theta)^{(i)}\,\dot{\theta} \tag{53}$$

where $\dot{\theta}$ is the rate of change of temperature in the material volume and $f_\beta\,(\theta)^{(i)}$ is the temperature dependent thermal expansion coefficient in each phase given by:

$$f_\beta(\theta)^{(i)} = \frac{\beta\,(\theta)^{(i)} - \beta_0^{(i)} b_\theta^{(i)}(\theta - \theta_0)}{1 - \beta\,(\theta)^{(i)}\,(\theta - \theta_0)} \qquad \beta\,(\theta)^{(i)} = \beta_0^{(i)}(1 - b_\theta^{(i)}(\theta - \theta_0)) \tag{54}$$

where $\beta_0^{(i)}$ is a thermal parameter fitted to experimental data. $\beta(\theta)^{(i)}$ is the functional form of the temperature dependence of the thermal expansion coefficient in each phase.

2.3. Multiphase Modeling - Interfacial stress formulation, polycrystalline approximation and transformation kinetics model

The transformation from austenite into martensite occurs via a shearing process. Here, we treat the interfacial stress in the same manner as the scalar hardening internal state variable κ, as acting in a non-directional manner. In a future work, we will utilize an orientation tensor to introduce the directionality of the interfacial (π) stress into the model, naturally incorporating the shearing aspects of the transformation process. The interfacial stress is determined to act in a manner where prior to the appearance of a second phase, the parent phase must experience a zero interfacial stress. This implies that the interfacial stress must ceases to evolve at a parent phase volume fraction value of unity. With the aforementioned mathematical requirements in mind and assuming a two phase system, the interfacial stress experienced by both the austenitic and martensitic phases is determined to be of the form:

$$\pi = c_\pi \frac{\Delta V}{V}\left[\phi - \phi^2\right] \tag{55}$$

where c_π is the interfacial stress parameter fitted to experimental data. $\frac{\Delta V}{V}$ is the change in lattice volume due to carbon addition given by:

$$\frac{\Delta V}{V} = \frac{V^{n+1} - V^n}{V^n} \qquad V = (3.548 + 0.44\%c)^3 \tag{56}$$

The resulting interfacial stress evolution equation is of the form:

$$\dot{\pi} = c_\pi \frac{\Delta V}{V}\left[\dot{\phi} - 2\phi\dot{\phi}\right] \tag{57}$$

The formulation of the interfacial stress evolution implemented here stipulates that communication between each phase is through an interaction stress π where each phase imposes its presence on all others and vise versa. This representative form of communication between each phase stipulates that the interaction between each phase is strictly through and resulting from each phases volume fraction, volume fraction rate and volume change. In the absence of an evolving volume fraction the interfacial stress ceases to evolve leading to a constant inter-phase interaction stress. In an attempt to satisfy the requirements of a polycrystalline model several techniques have been developed in the past to satisfy either equilibrium, compatibility or a combination of both. A Taylor [79, 80, 81] polycrystalline approximation (compatibility) requires uniform straining in all phases of a multiphase material. Therefore the elastic symmetric portion of the velocity gradient (Eqn. (29))in each phase becomes:

$$\mathbf{d}_e^{(i)} = \mathbf{d} - \mathbf{d}_p^{(i)} - \mathbf{d}_\theta^{(i)}. \tag{58}$$

For the case where there is negligible plasticity and thermal straining, the upper bound on the stress field is proportional to the symmetric portion of the velocity gradient:

$$\boldsymbol{\sigma}^{(i)} \propto \mathbf{d} \tag{59}$$

A Sachs [82] approximation requires proportional straining in all phases implying that the far-field forcing function is proportional to that experienced in each phase. For a two phase model, the austenite and martensite phases experience a stretch rate proportional to the far field strain rate:

$$\underbrace{\mathbf{d}^{(1)} = (1-\phi)\,\mathbf{d}}_{\textit{austenite strain rate}} \qquad \underbrace{\mathbf{d}^{(2)} = (\phi)\,\mathbf{d}}_{\textit{martensite strain rate}} \tag{60}$$

where $1-\phi$ represent the volume fraction of the austenite phase. For the case where $\phi = 0$ we recover a single phase model. When $\phi = 1$ a complete transformation in the material has occurred from austenite to martensite. Using a Sachs [82] argument, the coefficient of proportionality at the upper and lower bounds of the volume fraction must satisfy the constraint:

$$(1-\phi)\phi = 0 \tag{61}$$

mathematically enforcing a bound for the martensitic volume fraction ϕ such as:

$$0 \leq \phi \leq 1 \tag{62}$$

Budiansky and Wu [83] and a host of others as documented by Kocks et al. [84] developed a polycrystalline approximation technique that combines the benefits of both a Sachs and Taylor approach. Commonly referred to as a self-consistent approximation, it satisfies neither compatibility nor equilibrium but combines the physical features of both models. According to Knocks et al. [84], ‘self-consistent polycrystal models aim at deducing the overall response of the aggregate from the known properties of the constituent grains and an assumption concerning the interaction of each grain with its environment.’ With this in mind, we modify the requirements on the proportionality constants Eqn. (61) and replace the scalar volume fraction with a functional constraint:

$$(1 - f(\phi))f(\phi) = 0 \tag{63}$$

therefore the response of a satisfactory function $f(\phi)$ must satisfy the Eqn. (62). Therefore we can replace Eqn. (**??**) and Eqn. (**??**) with:

$$\underbrace{\mathbf{d}^{(1)} = (1 - f(\phi))\,\mathbf{d}}_{\textit{mod. austenite strain rate}} \qquad \underbrace{\mathbf{d}^{(2)} = (f(\phi))\,\mathbf{d}}_{\textit{mod. martensite strain rate}} \tag{64}$$

The efficacy of the multiphase model is dependent on the ability of each constituent part to capture the underlying physical behavior therefore implementing a physically based portioning algorithm is important.

We determine that a functional form that satisfies the constraint Eqn. (63) is sufficient; such as those used in determining a self-consistent approximation or as applied in percolation theory. We propose:

$$f(\phi) = \frac{1}{2}\left(1 + \tanh\left[c_{f1}\left(\phi - c_{f2}\right)\right]\right) \tag{65}$$

where c_{f1} determines the profile of the partitioning function. Analogous to inclusion used in material strengthening, further investigation will be directed towards determining the relationship between the shape parameter c_{f1} and martensitic spheroidal particles or platelets and how they affect the partitioning profile. The parameter c_{f2} is a transition parameter that determines the volume faction at which the martensite phase starts to experience the intensity of the strain field upon yielding of the softer austenite phase. The final set of evolution equations needed to complete the multiphase model is the phase kinetics evolution. As aforementioned, we are assuming a two phase system and qualitatively associate these phases with austenite to martensite; a non-diffusional type of transformation. The classical approach used to represent a non-diffusional transformation is the KM [50] kinetics model given by:

$$\dot{\phi} = -b_{km} \exp\left[-b_{km}\left(\theta_s - \theta\right)\right] U(\theta)\, \dot{\theta} \tag{66}$$

where b_{km} is a fixed parameter. θ_s is the temperature at which martensite starts forming determined using Andrews [85]. $U[\theta]$ is a unit step function given by:

$$U(\theta) = \begin{cases} 1 & \theta_f \leq \theta \leq \theta_s, \\ 0 & \text{else.} \end{cases} \tag{67}$$

where θ_f is the temperature at which martensite stops forming. For many reasons not limited to the notable burst in transformation rate analogous to a mathematical discontinuity [86], it has become necessary to develop alternative models. The KM [50] model is explicitly dependent on temperature rate and a fixed parameter $b_{km} = 0.011$. In other to circumvent the burst in transformation rate new models have been developed Lusk et al. [51, 67, 52]. These models are analogous in part to the transformation profile but with less of a discontinuous transformation rate. The non-diffusional kinetics model adopted here is that of Lusk et al. [51, 67, 52] where additional consideration was given to the carbon content influence on the transformation kinetics. Lusk's model for computing martensite's phase fraction (ϕ) is given by:

$$\dot{\phi} = -v\,(\%c)\,(\phi)^{a(\%c)}\,(1-\phi)^{b(\%c)}\, U(\theta)\, \dot{\theta} \tag{68}$$

where $\%c$ is the carbon content in percentage. $\dot{\theta}$ is the temprature rate. v, a, and b are transformation parameters fitted to dilatometry test. With initial conditions:

$$\phi(0) = 1E-5 \tag{69}$$

3. Results

3.1. Multiphase model evaluation - Parameter Identification

Parameter identification for the mechanical response of both the martensite and austenite phases was performed using a gradient based optimization routine following previous works of Marin et al. [73]. Table (1) is a list of the functional dependencies of mechanical and kinetics parameters. The material properties used here are that of SS304L table (3). Table (2) is a listing of 5120 Steel material constants. Figure (1a) and (1b) show EMMI model's mechanical response fitted to experimental data of 5120 austenite and martensite steel. Uniaxial tension tests for 5120 stainless steel were performed at a limited range of temperatures and strain rates.

Table 1: Material Parameters - Functional Dependencies

$\dot{\bar{\epsilon}}_p$-equation	$\dot{\boldsymbol{\alpha}}$-equation	$\dot{\kappa}$-equation	$\dot{\pi}$-equation	$\dot{\phi}$-equation
$f^{(i)} = c_2^{(i)} \exp\left(\frac{-Q_1^{(i)}}{\theta}\right)$	$r_d^{(i)} = c_3^{(i)} \exp\left(\frac{-Q_2^{(i)}}{\theta}\right)$	$R_d^{(i)} = c_3^{(i)} \exp\left(\frac{-Q_3^{(i)}}{\theta}\right)$	c_π	$\nu = \sum_{i=0}^{3} \nu_i \% c^i$
$n^{(i)} = \frac{c_9^{(i)}}{\theta} + c_1^{(i)}$	$h^{(i)} = c_4^{(i)}$	$H^{(i)} = c_6^{(i)}$		$a = \sum_{i=0}^{1} a_i \% c^i$
	$c_{\boldsymbol{\alpha}}^{(i)} = c_{11}^{(i)}$	$R_s^{(i)} = c_7^{(i)} \exp\left(\frac{-Q_4^{(i)}}{\theta}\right)$		$b = \sum_{i=0}^{1} b_i \% c^i$
		$Q_s^{(i)} = c_{10}^{(i)} \exp\left(\frac{-Q_5^{(i)}}{\theta}\right)$		
		$c_\kappa^{(i)} = c_{12}^{(i)}$		

Table 2: Material Parameters - 5120 Steel Constants

Contant	Austenite	Martensite
c_1	0.2074	5.8897
c_2	3.89E-10	9.36E-12
c_3	720940	370010
c_4	0.1090	0.1090
c_5	297.21	330.95
c_6	0.0011993	0.0470
c_7	0.0025771	0.11408
c_8	0.0001075	0.0055168
c_9	0.36714	1.6346
c_{10}	0	0
c_{11}	1.0	1.0
c_{12}	1.0	1.0
Q_1	0.2339	0.26523
Q_2	0.023787	0.045734
Q_3	2.1306	1.3961
Q_4	24.134	24.134
Q_5	0	0

Table 3: Material Parameters - Functional Dependencies

$\dot{\bar{\epsilon}}_p$-equation	$\dot{\boldsymbol{\alpha}}$-equation	$\dot{\kappa}$-equation	$\dot{\pi}$-equation	$\dot{\phi}$-equation
$f^{(i)} = c_2^{(i)} \exp\left(\frac{-Q_1^{(i)}}{\theta}\right)$	$r_d^{(i)} = c_3^{(i)} \exp\left(\frac{-Q_2^{(i)}}{\theta}\right)$	$R_d^{(i)} = c_3^{(i)} \exp\left(\frac{-Q_3^{(i)}}{\theta}\right)$	c_π	$\nu = \sum_{i=0}^{3} \nu_i \% c^i$
$n^{(i)} = \frac{c_9^{(i)}}{\theta} + c_1^{(i)}$	$h^{(i)} = c_4^{(i)}$	$H^{(i)} = c_6^{(i)}$		$a = \sum_{i=0}^{1} a_i \% c^i$
	$c_{\boldsymbol{\alpha}}^{(i)} = c_{11}^{(i)}$	$R_s^{(i)} = c_7^{(i)} \exp\left(\frac{-Q_4^{(i)}}{\theta}\right)$		$b = \sum_{i=0}^{1} b_i \% c^i$
		$Q_s^{(i)} = c_{10}^{(i)} \exp\left(\frac{-Q_5^{(i)}}{\theta}\right)$		
		$c_\kappa^{(i)} = c_{12}^{(i)}$		

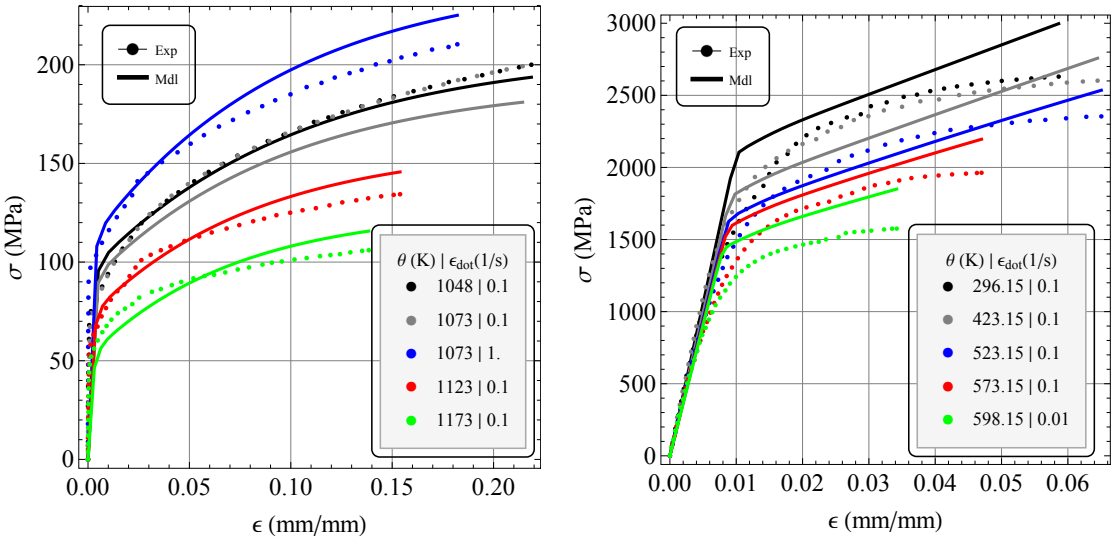

Fig. 1: Comparison of EMMI model response to experimental data for 5120 steel at various strain rates and temperatures. Figure (a): Experimental and numerical data and for 5120 steel austenite. Figure (b): Experimental and numerical data and for 5120 steel martensite.

3.2. Multiphase model evaluation - Polycrystalline approximation

A quantitative assessment of a Taylor, Sach and self-consistent polycrystalline approximation was carried with the help of a number of simplifying assumptions. We assumed isothermal conditions therefore material parameter and properties were evaluated at a fixed temperature. For the cases implemented here the material parameters were assumed to be a fit for a fixed carbon content, therefore:

$$\frac{\Delta V}{V} = 1. \tag{70}$$

Figure (2a) is strain rate as appropriated to each phase based on a Sachs, Taylor and a self-consistent polycrystalline approximation at a strain rate of $\dot{\epsilon} = 1/s$. The Taylor model, represented by the horizontal line at $\dot{\epsilon} = 1/s$, shows each phase experiences the same strain rate at all volume fractions of martensite. The Sachs model however, represented by a linear line through the origin, requires that each phase experiences a strain rate proportional to it's respective volume fractions. The self-consistent polycrystalline approximation using the constraint Eqn. (63) captures a more physical interaction between the mechanical properties of constituent phases.

For an assessment of the material response based on a Taylor, Sachs and self-consistent polycrystalline approximation three combinations of volume fraction ratios of both phases were tested. A combination of $90\%A + 10\%M$, $50\%A + 50\%M$ and $10\%A + 90\%M$ were used, where A and M stand for austenite and martensite. The resulting deviatoric stress field for all cases were determined using Eqn. (26). The parameter values chosen for the self-consistent approximation are $c_1 = 3.68$ and $c_2 = 0.5$.

At 10% martensite figure (2b), the self-consistent and Sachs models are expected to predict a similar deviatoric stress field. This is because the value of the proportionality functional in the self-consistent and Sachs are of very close. The result is physically meaningful because the stress field in general should not deviate much from a predominantly austenitic field irrespective of the material properties of the martensite. The disparity in the resulting deviatoric stress field from the Taylor model when compared with the Sachs and self-consistent is because both phases experience the same straining; this is in most cases non physical.

Similarly, at 50% martensite figure (2c), the self-consistent and Sachs approximations are expected to predict exactly the same magnitude of deviatoric stress field. This is because the transition parameter for the

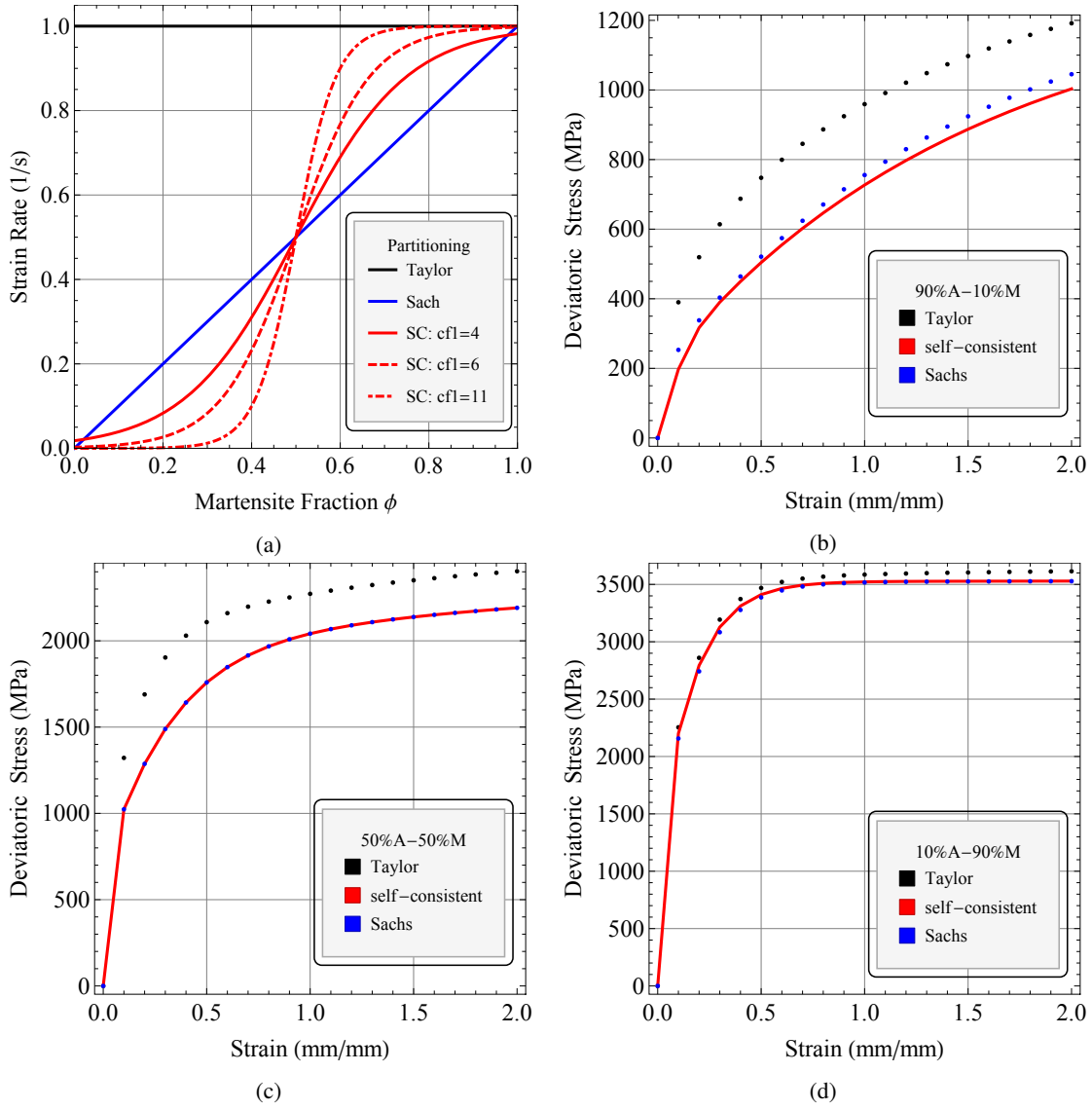

Fig. 2: Polycrystalline approximation. Figure (a): Strain rate partitioning as a function of martensite volume fraction based on a Sachs, Taylor and a self-consistent (sc) polycrystalline approximation at $\dot{\epsilon} = 1/s$. For the self-consistent model the parameter c_{f1} is 4, 6, 11 evaluated at $c_{f2} = 0.5$. Predicted deviatoric stress field using a Taylor, Sachs and self-consistent approximation: figure (b) at $90\%A + 10\%M$, figure (c) at $50\%A + 50\%M$, figure (d) at $10\%A + 90\%M$.

self-consistent approach was chosen to match exactly exactly at $\phi = 0.5$. The difference however with the Taylor assumption in emphasized by the difference in the internal state variable material parameter.

At 90% martensite figure (2d), there is very little distinction between a Taylor, Sachs or self-consistent approximation. For a self-consistent and Sachs approach the dominant strain rate in carried by the martensite which is naturally imposed using a Taylor approximation.

3.3. Multiphase model evaluation - Cooling rate and carbon content variation

A quantitative assessment of the multiphase EMMI material model coupled with the non-diffusive phase transformation kinetic model of Lusk et al. [51, 67, 52] was carried out. The parameters used for the transformation kinetics are published values based on previous works of Lusk et al. [51, 67, 52]. For the sake of simplicity material hardening dependence on carbon content was not accounted for. A evaluation of how the local thermal histories affect phase transformation was performed. Three multiphase EMMI material point simulation (mmps) runs were performed at 100C/s, 200C/s and 300C/s cooling rates. The transformation kinetics as depicted on figure (3a) shows a rapid transformation from austenite to martensite at higher cooling rates. As shown on figure (3b) and (3c) the deviatoric stress in the austenite and martensite phases increases as the transformation proceeds. Though these simulations only indicate the effect of cooling rate at a material point they qualitatively help to highlight how the deformation at juxtaposed material points would interact to cause deformation due to a temperature gradients. Figure (3d) shows the interfacial stress acting as a forward in the austenite and backward stress in the martensite phase. The simulation shows how the cooling rate controls the interfacial stress and consequentlythe transformation plasticity. Carbon content effect on the mechanical response was investigated. The transformation kinetics coupled with the multiphase EMMI model for a fixed cooling rate of 20/s at a carbon content ranging from 0.05% to 0.2%. Prantil et al. [86] determined that the rate of transformation was faster as the carbon content was increased. The results here show a similar qualitative behavior when coupled with the EMMI mechanical response. The field variables however show no change in the mechanical response. The transformation kinetics as depicted on figure (4a) the effect of carbon content on the transformation kinetics. The percentage of carbon content controls the smoothness of the rate of additional deformation due to transformation from austenite to martensite. Figure (4b) shows the additional straining induced by the transformation accounted for by the interfacial stress.Though these simulation only indicate the effect of carbon content locally, however they help qualitatively determine how carbon gradients at juxtaposed material points affect the transformation kinetics.

3.4. Multiphase model evaluation - Quenching BVP

The multiphase EMMI model coupled with the phase transformation kinetics model proposed by Lusk et al. [51, 67, 52] is applied to the case of a high aspect ratio annular rod (figure (5a)). In a high aspect ratio annular rod the temperature only varries in the radial direction. The inner and outer radius of the annular rod are 18mm and 56mm, respectively. In order to compute the thermal history of a high aspect ratio annular rod the one dimensional heat equation given by:

$$\dot{\theta} - k\nabla^2\theta = 0 \tag{71}$$

has to be solved for temperature field. k is the thermal diffusitivity coefficient of SS304L steel. The initial conditions of the one dimensional rod is such that:

$$\theta(t_0, r) = \begin{cases} 700\text{-}6\ Exp[r], & \text{if } r \leq 0 \\ 700\text{-}6\ Exp[-r], & \text{if } r \geq 0. \end{cases} \tag{72}$$

The boundary conditions at the inner and outer radii were prescribed to be at:

$$\theta(t, r_i) = 372.4\bar{1}, \qquad \theta(t, r_o) = 372.4\bar{1}. \tag{73}$$

Carbon content was chosen to be at $c = 0.2\%$ and therefore martensite start and finish temperatures were determined to be at $\theta_s = 650K$ and $\theta_f = 300K$. Figure (5b) shws the total deviatoric stress distribution at

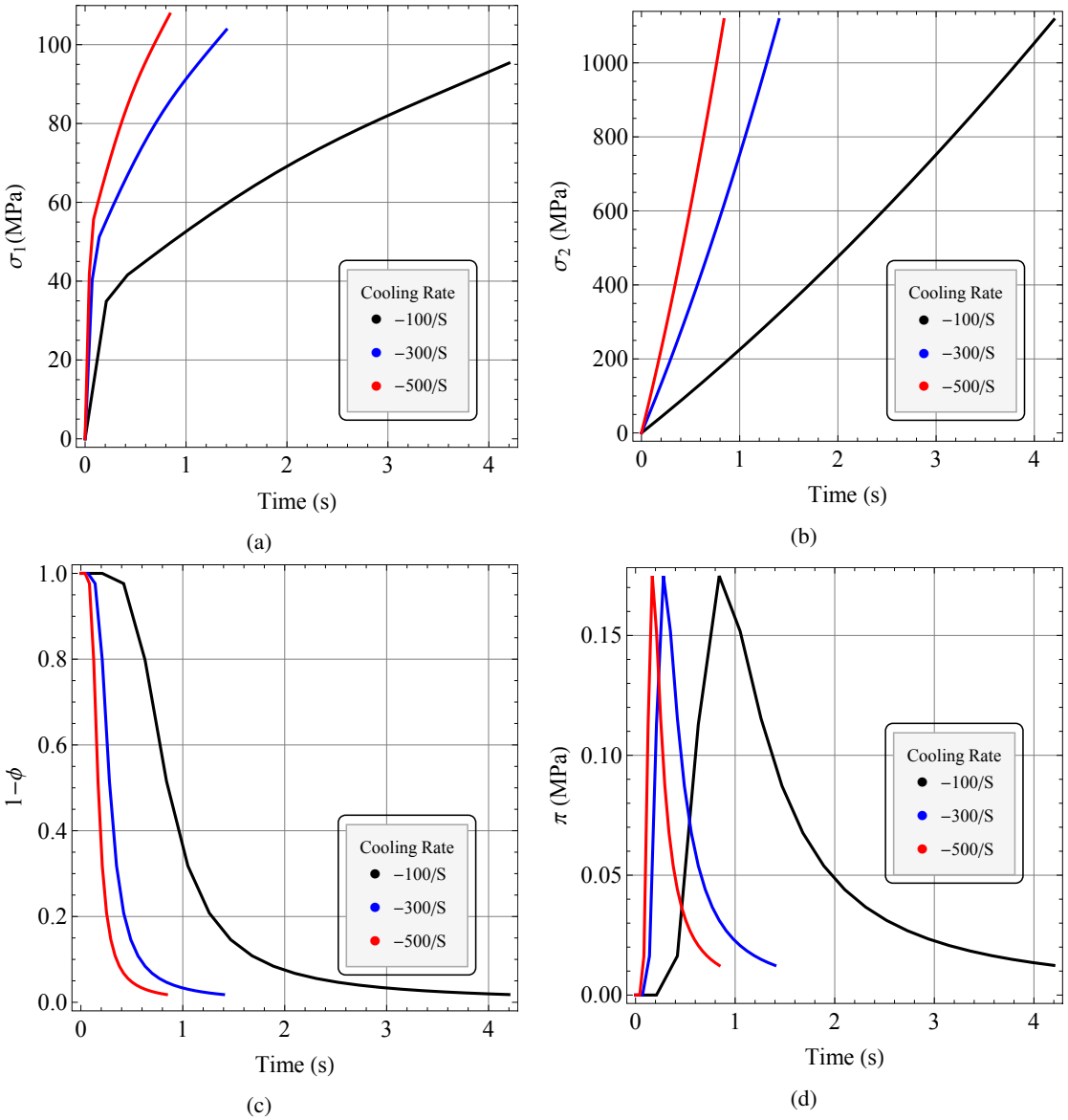

Fig. 3: Numerical evaluation of effects cooling rate. Multiphase EMMI model coupled with phase transformation kinetics model of Lusk et al. [51, 67, 52] evaluated at cooling rate 100C/s, 200C/s and 300C/s and 0.2% carbon content. Figure (a): Showing transformation kinetics from austenite to martensite. Figure (b): Showing the deviatoric stress in the austenite phase. Figure (c): Showing the deviatoric stress in the martensite phase. Figure (d): Showing the interfacial stress acting as a forward and backward stress in the austenite and martensite phases respectively.

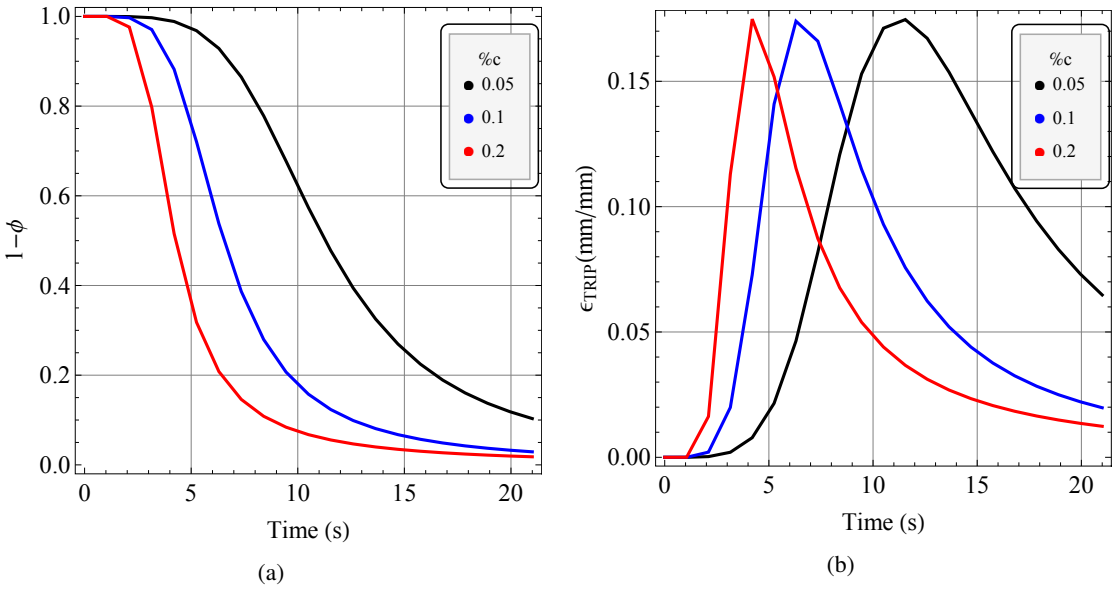

Fig. 4: Numerical evaluation of effects carbon content. Multiphase EMMI model coupled with phase transformation kinetics model of Lusk et al. [51, 67, 52] evaluated at 0.05%, 0.1% and 0.2% carbon content and 20C/s. Figure (a): Showing the kinetics of transformation from austenite to martensite. Figure (b): Showing the TRIP strain computed using the interfacial stress acting in the austenite and martensite phases, respectively.

evenly spaced radial locations after 300 and 600 seconds after quenching. The results captures the overall expected behavior given that the initial radial temperature distribution was specified to be at the maximum midway between the inner and outer radii; $\theta_{max} = \theta(t = 0, x = 36mm)$. The volume fraction distribution along the radius after 300 and 600 seconds indicate that the areas along the radius of the annular rod with a higher volume fraction of martensite in turn have larger residual stresses. This is quantitatively correct given that the mechanical properties of the martensite is an order of magnitude larger than that of austenite.

Figure (5c) and (5d) shows the total deviatoric stress along side with martensite volume fraction at evenly spaced radial locations after 300 and 600 seconds evaluated with and without accounting for transformation plasticity. The results highlights the significance of account for transformation plasticity. At 300 seconds (figure (5c)), the transformations kinetics does not have a pronounced effect when compared to a later time (figure (5d)) during the quench. The difference in the magnitude of the stresses with and without accounting for TRIP becomes significant as martensite's volume fraction locally dominates the parent austenite. The quantity of the martensitic platelets are insignificant at (figure (5c)) and therefore not enough to overwhelm the overall internal state of the bulk/parent austenite. This feature highlights the volume fraction sensitivity of the multiphase EMMI inelasticity model. The sustainability of an internal state variable model as a viable option for modeling multiphase material lies in its ability to accurately capture the physics of the internal state of a multiphase body.

4. Summary

The EMMI single phase internal state variable model was extended to accommodate the presence of product phases. We assumed a two-phase system where the mechanical response and transformation kinetics model for austenite and martensite were qualitatively associated with austenite and martensite. Available is experimental data of 5120 steel over a limited strain rate and temperature regime.

The additional TRIP was accounted for through the introduction of a physically appropriate interfacial stress acting as a forward stress in the softer austenite, and a backward stress in the martensite. Since the

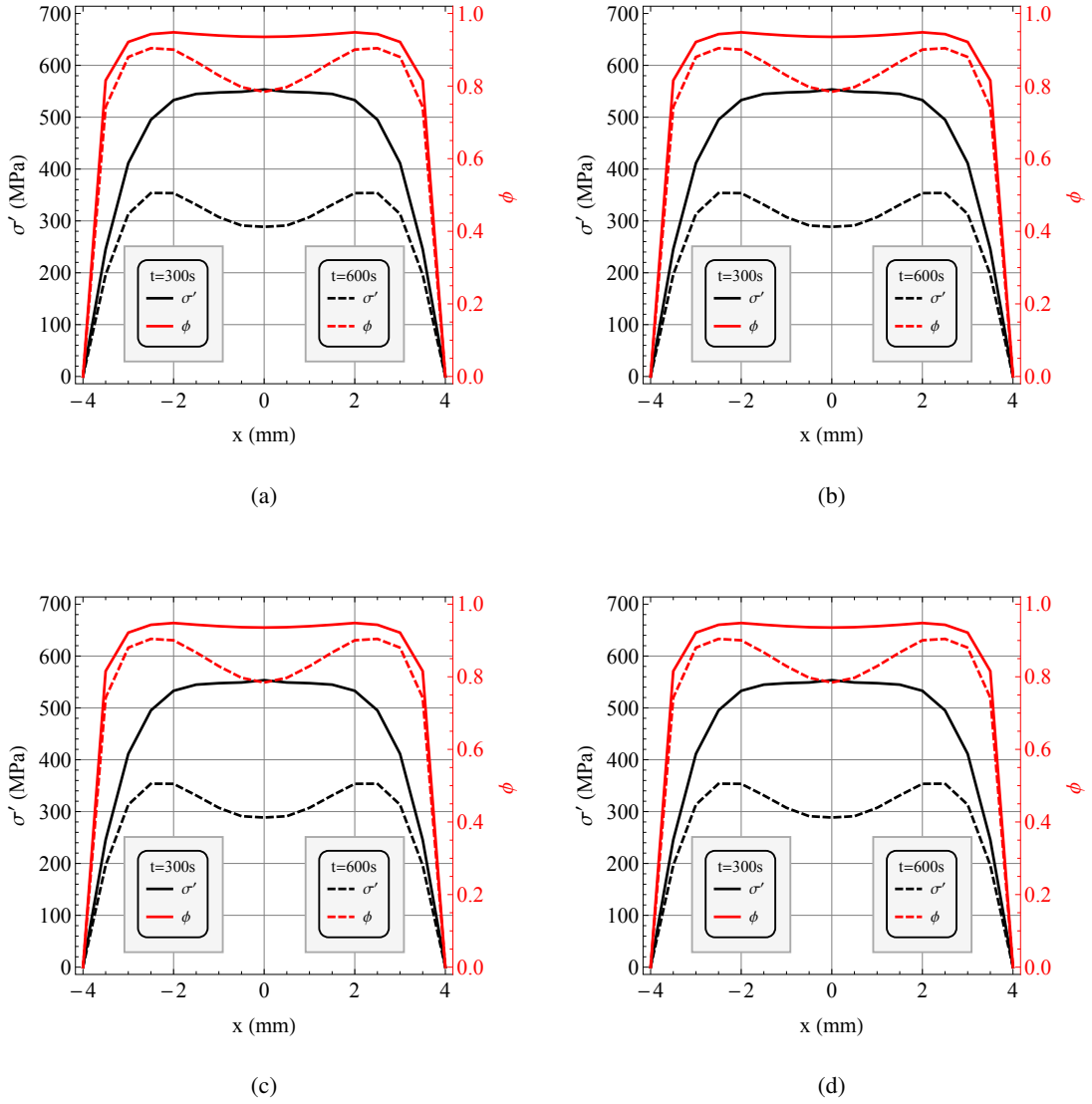

Fig. 5: Numerical evaluation of quenching BVP. Multiphase EMMI model coupled with the phase transformation kinetics model of Lusk et al. [51, 67, 52] applied to the quenching of a long annular rod. Figure (a): Showing dimensions of high aspect ratio annular rod. Figure (b): Showing the $\acute{\boldsymbol{\sigma}}_{total}$ and ϕ distribution along the radius after 300 and 600 seconds. Figure (c): Showing the $\acute{\boldsymbol{\sigma}}_{total}$ and ϕ distribution along the radius after 300(s) with and without accounting for transformation plasticity. Figure (d):Showing the $\acute{\boldsymbol{\sigma}}_{total}$ and ϕ distribution along the radius after 600(s) with and without accounting for transformation plasticity.

efficacy of a multiphase model is dependent on its ability to capture the behavior of constituents phases and their subsequent interaction, we introduce a physically based self-consistent partitioning algorithm. A quantitative assessment of the material response and plastic flow based on the Taylor, Sachs and self-consistent approximation was carried out.

References

[1] C. Truesdell, W. Noll, The Non-Linear Field Theories of Mechanics, Springer-Verlag, 1992.
[2] C. Truesdell, W. Noll, The non-linear field theories of mechanics, Springer, 2004.
[3] B. D. Coleman, W. Noll, The thermodynamics of elastic materials with heat conduction and viscosity, Archive for Rational Mechanics and Analysis 13 (1) (1963) 167–178.
[4] B. D. Coleman, V. J. Mizel, Existence of caloric equations of state in thermodynamics, The Journal of Chemical Physics 40 (1964) 1116.
[5] B. D. Coleman, M. E. Gurtin, Thermodynamics with internal state variables, The Journal of Chemical Physics 47 (1967) 597.
[6] J. D. Eshelby, The determination of the elastic field of an ellipsoidal inclusion, and related problems, Proceedings of the Royal Society A Mathematical Physical and Engineering Sciences 241 (1226) (1957) 376–396.
[7] J. D. Eshelby, The elastic field outside an ellipsoidal inclusion, Proceedings of the Royal Society of London Series A Mathematical and Physical Sciences 252 (1271) (1959) 561–569.
[8] J. Ericksen, Equilibrium of bars, Journal of Elasticity 5 (1975) 191–201.
[9] J. Ball, Existence of solutions in finite elasticity, in: Proceedings of the IUTAM Symposium on Finite Elasticity, Springer, 1982, pp. 1–12.
[10] E. Bain, The nature of solid solutions, Chem. Metall. Eng 28 (1923) 21–24.
[11] M. S. Wechsler, On the Theory of the Formation of Martensite., 1954.
[12] K. Tanaka, S. Nagaki, A thermomechanical description of materials with internal variables in the process of phase transitions, Ingenieur-Archiv 51 (5) (1982) 287–299.
[13] J.-B. Leblond, G. Mottet, J. Devaux, A theoretical and numerical approach to the plastic behaviour of steels during phase transformations - i. derivation of general relations, Journal of the Mechanics and Physics of Solids 34 (4) (1986) 395–409.
[14] J. Leblond, G. Mottet, J. Devaux, A theoretical and numerical approach to the plastic behaviour of steels during phase transformationsii. study of classical plasticity for ideal-plastic phases, Journal of the Mechanics and Physics of Solids 34 (4) (1986) 411–432.
[15] R. Hill, The essential structure of constitutive laws for metal composites and polycrystals, Journal of the Mechanics and Physics of Solids 15 (2) (1967) 79–95.
[16] J. Mandel, Contribution théorique à l'étude de l'écrouissage et des lois de l'écoulement plastique, in: Proc. 11th Int. Congr. Appl. Mech, 1964, pp. 502–509.
[17] J. B. Leblond, J. Devaux, J. C. Devaux, Mathematical modeling of transformation plasticity in steels i: Case of ideal-plastic phases, International Journal of Plasticity 5 (1989) 551–572.
[18] J. B. Leblond, J. Devaux, J. C. Devaux, Mathematical modeling of transformation plasticity in steels II: Coupling with strain hardening phenomena, International Journal of Plasticity 5 (1989) 573–591.
[19] J. Leblond, Simulation num é america welding - mod é lity math é matic transformations m é tallurgiques - state works progress, Tech. rep., Technical Report TM / C DC/80.066, Framatome (1980).
[20] J. Giusti, Contraintes et déformations résiduelles d'origine thermique: application au soudage et à la trempe des aciers, Ph.D. thesis (1981).
[21] C. L. Magee, Transformation Kinetics,Microplasticity and Aging of Martensite in Fe-31 Ni, Carnegie Institute of Technology, 1966.
[22] G. W. Greenwood, R. H. Johnson, The Deformation of Metals Under Small Stresses During Phase Transformations, Proceedings of The Royal Society of London. Series A, Mathematical and Physical Sciences (1934-1990) 283 (1965) 403–422.
[23] D. Gigou, Plasticité de transformation: Cas de la transformation martensitique, 1985.
[24] F. Abrassart, Influence des transformations martensitiques sur les propriétés mécaniques des alliages du système fe-ni-cr-c, PhD Report, Université de Nancy, France.
[25] W. Mitter, Umwandlungsplastizit "a t and Ber ü cksichtigung in the calculation of residual stresses, Borntraeger-Verlag, 1987.
[26] D. J. Bammann, Modeling temperature and strain rate dependent large deformations of metals, Applied Mechanics Reviews 43 (1990) 312.
[27] D. J. Bammann, V. C. Prantil, J. F. Lathrop, A plasticity model for materials undergoing phase transformations, Simulation of Materials Processing: Theory, Methods and Applications. NUMIFORM 95. (1995) 219 224.
[28] D. Bammann, M. Chiesa, G. Johnson, Modeling large deformation and failure in manufacturing processes, Theoretical and Applied Mechanics (1996) 359–376.
[29] D. Bammann, M. Chiesa, G. Johnson, Modeling large deformation and failure in manufacturing processes, in: Theoretical and Applied Mechanics 1996: Proceedings of the XIXth International Congress of Theoretical and Applied Mechanics, Kyoto, Japan, 25-31 August 1996, Vol. 19, North Holland, 1997, p. 359.
[30] M. Ashby, The deformation of plastically non-homogeneous materials, Philosophical Magazine 21 (170) (1970) 399–424.
[31] D. Bammann, V. Prantil, A. Kumar, Development of a carburizing and quenching simulation tool: a material model for low carbon steels undergoing phase transformations, Tech. rep., Lawrence Livermore National Lab., CA (United States) (1996).
[32] A. Khan, S. Huang, Continuum Theory of Plasticity, Wiley-Interscience publication, Wiley, 1995.

[33] N. Böck, G. Holzapfel, A large strain continuum and numerical model for transformation induced plasticity (trip), in: Fifth World Congress on Computational Mechanics, pages–, Austria, 2002.
[34] E. Kroner, Allgemeine kontinuumstheorie der versetzungen, Arch, 1960.
[35] E. H. Lee, D. T. Liu, Finite strain plasticity particularly for plane waves, Journal of Applied Physics 38.
[36] H. Hallberg, P. Hkansson, M. Ristinmaa, A constitutive model for the formation of martensite in austenitic steels under large strain plasticity, International Journal of Plasticity 23 (7) (2007) 1213 – 1239.
[37] D. Tjahjanto, S. Turteltaub, A. Suiker, Crystallographically based model for transformation-induced plasticity in multiphase carbon steels, Continuum Mechanics and Thermodynamics 19 (7) (2008) 399–422.
[38] R. Stringfellow, D. Parks, G. Olson, A constitutive model for transformation plasticity accompanying strain-induced martensitic transformations in metastable austenitic steels, Acta Metallurgica et Materialia 40 (7) (1992) 1703–1716.
[39] S. Sjostrom, The calculation of quench stresses in steel, Ph.D. thesis, Linkoping Univeristy, Sweden (1982).
[40] S. Sjostrom, Interactions and constitutive models for calculating quench stresses in steel, Materials Science and Technology 1 (1985) 823–829.
[41] Z. Bo, D. C. Lagoudas, Thermomechanical modeling of polycrystalline smas under cyclic loading, part i: theoretical derivations, International Journal of Engineering Science 37 (9) (1999) 1089 – 1140.
[42] V. I. Levitas, Thermomechanical theory of martensitic phase transformations in inelastic materials, International Journal of Solids and Structures 35 (910) (1998) 889 – 940.
[43] V. I. Levitas, D. L. Preston, Three-dimensional landau theory for multivariant stress-induced martensitic phase transformations .i. austenite to martensite, Phys. Rev. B 66 (2002) 134206.
[44] V. I. Levitas, D. L. Preston, Three-dimensional landau theory for multivariant stress-induced martensitic phase transformations. ii. multivariant phase transformations and stress space analysis, Physical Review B 66 (13) (2002) 134207.
[45] W. A. Johnson, R. F. Mehl, Reaction kinetics in processes of nucleation and growth, Trans. Aime 135 (8) (1939) 396–415.
[46] M. Avrami, Kinetics of phase change. i general theory, The Journal of Chemical Physics 7 (12) (1939) 1103–1112.
[47] M. Avrami, Kinetics of phase change. ii transformation-time relations for random distribution of nuclei, The Journal of Chemical Physics 8 (2) (1940) 212–224.
[48] M. Avrami, Granulation, phase change, and microstructure kinetics of phase change iii, The Journal of Chemical Physics 9 (2) (1941) 177–184.
[49] A. Kolmogorov, On the Statistical Theory of Metal Crystallization, Izv. Akad. Nauk SSSR, Ser. Math 1 (1937) 335–360, computes density of fairly general Johnson-Mehl crystals and the probability that a point is not in a crystal yet.
[50] D. Koistinen, R. Marburger, A simplified procedure for calculating peak position in x-ray residual stress measurements on hardened steel, Trans. ASM 51 (1959) 537.
[51] M. Lusk, G. Krauss, H.-J. Jou, A balance principle approach for modeling phase transformation kinetics, Le Journal de Physique IV 5 (C8) (1995) C8–279.
[52] M. Lusk, H.-J. Jou, On the rule of additivity in phase transformation kinetics, Metallurgical and Materials Transactions A 28 (2) (1997) 287–291.
[53] M. T. Lusk, Y.-K. Lee, A global material model for simulating the transformation kinetics of low alloy steels, in: 7 th International Seminar of IFHT(International Federation for Heat Treatment and Surface Engineering), 1999, pp. 273–282.
[54] B. L. Ferguson, A. M. Freborg, G. Petrus, M. L. Callabresi, Predicting the heat-treat response of a carburized helical gear., Gear Technology 19 (6) (2002) 20–25.
[55] B. L. Ferguson, Z. Li, A. Freborg, Modeling heat treatment of steel parts, Computational Materials Science 34 (3) (2005) 274–281.
[56] A. S. U. Manual, version 5.7, 1997. hibbitt, karlsson and sorensen, Inc., Providence, Rhode Island.
[57] V. S. Warke, Predicting the response of powder metallurgy steel components to heat treatment, Ph.D. thesis, Worcester Polytechnic Institute (2008).
[58] S. Zhang, Z. Li, B. L. Ferguson, Effect of carburization on the residual stress and fatigue life of a transmission shaft, in: Heat Treating: Proceedings of the 23rd Heat Treating Society Conference, September 25-28, 2005, David L. Lawrence Convention Center, Pittsburgh, Pennsylvania, ASM International (OH), 2006.
[59] Z.-c. Li, B. Ferguson, Computer modeling and validations of steel gear heat treatment processes using commercial software dante, Journal of Shanghai Jiaotong University (Science) 16 (2) (2011) 152–156.
[60] Z. Li, A. Freborg, B. Hansen, T. Srivatsan, Modeling the effect of carburization and quenching on the development of residual stresses and bending fatigue resistance of steel gears, Journal of Materials Engineering and Performance 22 (3) (2013) 664–672.
[61] T. Inoue, D.-Y. Ju, K. Arimoto, Metallo-thermo-mechanical simulation of quenching process–theory and implementation of computer code" hearts", Quenching and Distortion Control (1992) 205–212.
[62] T. Inoue, K. Arimoto, Development and implementation of cae system hearts for heat treatment simulation based on metallo-thermo-mechanics, Journal of Materials Engineering and Performance 6 (1) (1997) 51–60.
[63] S. R. Institute, Farmatome, SYSWELD-A Predictive Model for Heat Treat Distortion, Presentation at the National Centerfor Manufacturing Sciences, Ann Arbor, Michigan, April 14, 1992.
[64] J. N., S. S., Current Status of TRAST: A Material Model Subroutine System for the Calculation of Quench Stressesin Steel,ABAQUS Users Conference Proceedings, 1993.
[65] A. Comsol, Comsol multiphysics users guide, Version: September.
[66] S. U. Manual, version sp3. 1, Dassault Systemes, Sureness, France.
[67] H.-J. Jou, M. T. Lusk, Comparison of johnson-mehl-avrami-kologoromov kinetics with a phase-field model for microstructural evolution driven by substructure energy, Physical Review B 55 (13) (1997) 8114.
[68] D. Bammann, V. Prantil, A. Kumar, J. Lanthrop, D. Mosher, M. Lusk, H.-J. Jou, G. Krauss, W. Elliott, A material model for low carbon steels undergoing phase transformations, In: Totten G, Proceedings of the Second International Conference on Quenching

and the Control of Distortion. Warrendale, PA, 1996.
[69] D. Bammann, V. Prantil, J. Lathrop, A model of phase transformation plasticity, Modelling of Casting, Welding and Advanced Solidification Processes VII (1995) 275–285.
[70] D. A. . B. Hughes, D. J. . Godfrey, W. . P. Andrew, V. C. . Holm, Elizabeth, Capturing recrystallization of metals with a multi-scale materials model, Sandia Report SAND2000-8232, Sandia National Laboratories, Livermore, CA, 2000.
[71] D. J. . M. Bammann, D. A. . Hughes, D. A. . Moody, N. R. . Dawson, Paul, Using spatial gradients to model localization phenomena, Sandia Report SAND99-8588, Sandia National Laboratories, Livermore, CA, 1999.
[72] M. E. Gurtin, Generalized ginzburg-landau and cahn-hilliard equations based on a microforce balance, Physica D: Nonlinear Phenomena 92 (3) (1996) 178–192.
[73] E. B. Marin, D. J. Bammann, R. A. Regueiro, G. C. Johnson, On the Formulation, Parameter Identification and Numerical Integration of the EMMI Model: Plasticity and Isotropic Damage, SAN D2006-0200, Sandia National Laboratories, 2006.
[74] H. J. Frost, M. F. Ashby, Deformation mechanism maps: the plasticity and creep of metals and ceramics.
[75] C. O. Frederick, P. Armstrong, A mathematical representation of the multiaxial bauschinger effect, Materials at High Temperatures 24 (1) (2007) 1–26.
[76] U. Kocks, H. Mecking, A mechanism for static and dynamic recovery, Strength of metals and alloys (1980) 345–350.
[77] Y. Estrin, H. Mecking, A unified phenomenological description of work hardening and creep based on one-parameter models, Acta Metallurgica 32 (1) (1984) 57–70.
[78] E. Nes, Recovery revisited, Acta Metallurgica et Materialia 43 (6) (1995) 2189 – 2207. doi:http://dx.doi.org/10.1016/0956-7151(94)00409-9.
URL http://www.sciencedirect.com/science/article/pii/0956715194004099
[79] G. Taylor, U. Dehlinger, Strains in crystalline aggregate, in: R. Grammel (Ed.), Deformation and Flow of Solids / Verformung und Fliessen des Festkrpers, International Union of Theoretical and Applied Mechanics / Internationale Union fr Theoretische und Angewandte Mechanik, Springer Berlin Heidelberg, 1956, pp. 3–12.
[80] G. I. Taylor, Plastic strain in metals, 1938.
[81] G. Taylor, Analysis of plastic strain in a cubic crystal, Stephen Timoshenko 60th Anniversary Volume (1938) 218–224.
[82] G. Sachs, Zur ableitung einer fliebedingung, in: Mitteilungen der deutschen Materialprfungsanstalten, Springer Berlin Heidelberg, 1929, pp. 94–97.
[83] B. Budiansky, T. Te Wu, Theoretical prediction of plastic strains of polycrystals, Contract Nonr 1866(02) Technical report, Division of Engineering and Applied Physics, Harvard University, 1961.
[84] U. Kocks, C. Tomé, H. Wenk, H. Mecking, Texture and Anisotropy: Preferred Orientations in Polycrystals and their Effect on Materials Properties, Cambridge University Press, 2000.
[85] K. W. Andrew, JIST 203 (1965) 721–727.
[86] V. C. Prantil, M. L. Callabresi, J. F. Lathrop, G. S. Ramaswamy, M. T. Lusk, Simulating distortion and residual stresses in caburized thin strips, Journal of Engineering Materials and Technology 125 (2003) 116–124.